

# Radioactively-Powered Gamma-Ray Transient Associated with a Kilonova from Neutron Star Merger

Meng-Hua Chen<sup>1</sup>, Rui-Chong Hu<sup>1</sup>, En-Wei Liang<sup>\*1</sup>

## ABSTRACT

Association of GW170817/GRB170817A/AT2017gfo provides the first direct evidence for neutron star mergers as significant sources of  $r$ -process nucleosynthesis. A gamma-ray transient (GRT) would be powered by the radioactive decay of the freshly-synthesized  $r$ -process elements. By analyzing the composition and gamma-ray opacity of the kilonova ejecta in details, we calculate the lightcurve and spectrum of the GRT for a spherically symmetric merger ejecta with mass  $M_{\text{ej}} = 0.001 \sim 0.05 M_{\odot}$  and expansion velocity  $v_{\text{ej}} = 0.1 \sim 0.4c$ . It is found that the peak of the GRT lightcurve depends on  $M_{\text{ej}}$  and  $v_{\text{ej}}$  as  $t_{\text{pk}} \approx 0.9 \text{ days } (M_{\text{ej}}/0.01 M_{\odot})^{1/2} (v_{\text{ej}}/0.2c)^{-1}$  and  $L_{\text{pk}} \approx 7.0 \times 10^{40} \text{ erg s}^{-1} (M_{\text{ej}}/0.01 M_{\odot})^{1/2} (v_{\text{ej}}/0.2c)$ . Most radiating photons are in the 100 – 3000 keV band and the spectrum peaks at round 800 keV for different nuclear physics inputs. The line features are blurred out by the Doppler broadening effect and the uncertainties of nuclear physics data. Adopting the ejecta parameters reported in literature, we examine the detection probability of the possible GRT associated with AT2017gfo. We show that the GRT cannot be convincingly detected with the proposed missions in the MeV band, such as ETCC and AMEGO. The low gamma-ray flux, together with the extremely low event rate at local universe, makes a great challenge for discovery of the GRTs.

*Subject headings:* Gamma-ray burst; Explosive nucleosynthesis; Gravitational wave sources

## 1. Introduction

Kilonova powered by neutron-rich ejecta from merger of binary neutron stars was theoretically predicted and observationally confirmed (Lattimer & Schramm 1974; Abbott et

---

<sup>1</sup>Guangxi Key Laboratory for Relativistic Astrophysics, School of Physical Science and Technology, Guangxi University, Nanning 530004, People's Republic of China; lew@gxu.edu.cn

al. 2017a,b). Heavy elements beyond iron are synthesized through the rapid neutron capture process (*r*-process; Burbidge et al. 1957) in the expanding merger ejecta. The radioactive decay of *r*-process elements produces a characteristic electromagnetic transient in the ultraviolet/optical/near-infrared wavelengths, which is known as a “kilonova” (Li & Paczyński 1998; Metzger et al. 2010; Korobkin et al. 2012; Barnes & Kasen 2013; Kasen et al. 2013; Barnes et al. 2016; see Metzger 2019 for a recent review). The first unambiguous kilonova, named AT2017gfo, was discovered on 2017 August 17 (Abbott et al. 2017b; Arcavi et al. 2017; Chornock et al. 2017; Coulter et al. 2017; Cowperthwaite et al. 2017; Drout et al. 2017; Evans et al. 2017; Kasliwal et al. 2017; Nicholl et al. 2017; Pian et al. 2017; Smartt et al. 2017; Tanvir et al. 2017). This kilonova followed a gravitational-wave signal compatible with the inspiral and coalescence of binary neutron stars (GW170817, Abbott et al. 2017a). The luminosity and color evolution of AT2017gfo suggest the presence of two distinct components: an early “blue” component driven by wind ejecta and a later “red” component driven by the dynamical ejecta (Kasen et al. 2017; Kilpatrick et al. 2017; Nicholl et al. 2017; Tanaka et al. 2017; Tanvir et al. 2017; Troja et al. 2017; Villar et al. 2017). The blue component is attributed to the ejecta dominated by light *r*-process nuclei (atomic mass number  $A \lesssim 140$ ), while the red component is likely from the ejecta rich in lanthanides and heavy *r*-process material ( $A \gtrsim 140$ ). These observational features are well consistent with the theoretical expectation. The absorption features in the kilonova spectrum may be used to identify specific heavy elements. However, due to the large Doppler shift and blend of many absorption lines, no individual heavy elements have been identified except for strontium (atomic number  $Z = 38$ ) in the observed spectra of AT2017gfo (Watson et al. 2019).

Besides the kilonova, a gamma-ray transient (GRT) would be also powered by the radioactive decay of freshly-synthesized heavy elements (Hotokezaka et al. 2016). Radioactive decay of unstable nuclei are usually left the daughter nucleus in an excited state. The subsequent decay of the daughter nucleus to a lower-energy state results in gamma-ray emission in specific energy. Detection of these gamma-ray photons can provide conclusive evidence for identifying individual elements and tracking their evolution. Radioactive gamma-ray emission from neutron star mergers was studied by several groups. They focused on identifying the gamma-ray line features associated with *r*-process elements (Li 2019; Wu et al. 2019a; Korobkin et al. 2020; Chen et al. 2021). For instance, Chen et al. (2021) showed that the decay chain of  $^{132}\text{Te}$  ( $t_{1/2} = 3.21$  days)  $\rightarrow$   $^{132}\text{I}$  ( $t_{1/2} = 0.10$  days)  $\rightarrow$   $^{132}\text{Xe}$  would produce several bright gamma-ray lines in the MeV band and would be marginally detectable with the future gamma-ray detector if the source is at a distance of 40 Mpc. Note that the characteristics of a GRT and associated kilonova are sensitive to the ejecta properties, especially the mass and expansion velocity. Recent numerical simulations of binary neutron star mergers show

that the ejecta mass may be in a range from  $\sim 0.001M_\odot$  to nearly  $0.05M_\odot$ , which depends strongly on the total mass, mass ratio of binary system, and neutron star equation of state (Bauswein et al. 2013; Hotokezaka et al. 2013; Sekiguchi et al. 2016; Dietrich et al. 2017; Fujibayashi et al. 2018; Radice et al. 2018; Shibata & Hotokezaka 2019; Nedora et al. 2021). The typical velocity of the ejecta is in the sub-relativistic regime,  $\sim 0.1 - 0.4c$ , where  $c$  is the speed of light. Investigation the GRTs and kilonovae in such plausible ranges would be helpful for accessing their delectability with current and upcoming telescopes.

The opacities of  $r$ -process elements also play an important role in deriving the lightcurve and spectrum of a GRT. Korobkin et al. (2020) studied the gamma-ray emission by simply assuming that all heavy  $r$ -process elements have an opacity comparable to the iron element. Since the probability of photoelectric absorption is proportional to the atomic number as  $Z^4$ , the opacities of  $r$ -process elements are significantly higher than those of the iron element. The higher opacities will lead to the gamma-ray photons suffer stronger absorption, hence dimmer luminosity.

This paper studies the GRTs from neutron star mergers in reasonable ranges based on numerical results by considering the opacities of  $r$ -process elements in detail, in which the opacity is estimated based on the detailed nuclide composition obtained from nucleosynthesis calculations of the  $r$ -process. In Section 2, we study the composition and gamma-ray opacity in detail. Section 3 presents the model and our numerical results for deriving the GRTs with mass ranging in  $M_{\text{ej}} = 0.001 \sim 0.05M_\odot$  and the expansion velocity in  $v_{\text{ej}} = 0.1 \sim 0.4c$ . As a case study, we apply our model to the possible GRT associated with AT2017gfo for evaluating its detection probability in Section 4. Conclusions and discussion are presented in Section 5.

## 2. Composition and Gamma-ray Opacity of the Merger Ejecta

### 2.1. Ejecta Model

We assume the merger ejecta is spherical and expanding homogenously, and the ejected material is a sum of two components, i.e. a neutron-rich dynamical ejecta generated by tidal disruption and a wind ejecta driven by the post-merger remnant. The merger ejecta is considered consist of an ensemble of a series of mass layers and each layer evolves nearly independently with a constant velocity  $v_n$ . We use a power-law mass density profile of the merger ejecta (Zhu et al. 2021),

$$\rho_{\text{ej}}(v_n, t) = \left(\frac{3}{4\pi}\right) \frac{M_{\text{ej}}}{v_n^3 t^3} \left(\frac{v_n}{v_0}\right)^{-3}, \quad (1)$$

where  $M_{\text{ej}}$  is the total ejecta mass,  $v_0$  is the average velocity. We vary the ejecta masses and expansion velocities of each ejecta component over the range  $M_{\text{ej}} = 0.001 - 0.05 M_{\odot}$  and  $v_{\text{ej}} = 0.1 - 0.4c$ , covering the ranges of ejecta parameters reported in the literature (Bauswein et al. 2013; Hotokezaka et al. 2013; Sekiguchi et al. 2016; Dietrich et al. 2017; Fujibayashi et al. 2018; Radice et al. 2018; Shibata & Hotokezaka 2019; Nedora et al. 2021).

## 2.2. Composition

To obtain the detailed composition of  $r$ -process materials, we employ the nuclear reaction network code SkyNet for  $r$ -process simulations (Lippuner & Roberts 2015, 2017). The code presents the evolutions of the abundances for 7843 nuclides, ranging from free neutrons and protons to  $^{337}\text{Cn}$  ( $Z = 112$ ), and includes over 140,000 nuclear reactions. The strong reaction rates are taken from the JINA REACLIB database (Cyburt et al. 2010) and the inverse rates are computed from detailed balance. In our calculations, we use the state-of-the-art nuclear physics inputs, including the experimental masses from the latest Atomic Mass Evaluation (AME2020, Wang et al. 2021) and experimental data from newly published database NUBASE2020 (Kondev et al. 2021). For the nuclide species without experimental data, we use the theoretical data from Finite-Range Droplet Model (FRDM, Möller et al. 2016). The neutron capture rates are calculated with each associated mass data using the nuclear reaction code TALYS (Goriely et al. 2008). For spontaneous fission, neutron-induced fission and  $\beta$ -delayed fission, we use the double Gaussian fission fragment distributions from Kodama-Takahashi model (KT, Kodama & Takahashi 1975). We note that the choice of nuclear physics models and fission fragment distributions has significant impact on the  $r$ -process nucleosynthesis simulations (Mumpower et al. 2018; Zhu et al. 2021).

In our two-component model, the dynamical ejecta is calculated with entropy  $s = 10 k_B/\text{baryon}$ , expansion timescale  $\tau_{\text{dyn}} = 10$  ms, and electron fraction  $Y_e \sim 0.05 - 0.25$  (with increments of 0.01). For a wind ejecta, we take  $s = 20 k_B/\text{baryon}$ ,  $\tau_{\text{dyn}} = 30$  ms, and  $Y_e \sim 0.20 - 0.40$  (with increments of 0.01). Following Wu et al. (2019b), we assume that the ejected material contains a Gaussian  $Y_e$  distribution characterized by a central value  $Y_{e,c}$  and a width  $\Delta Y_e$ , i.e.,

$$Y_i(t) = \int Y_i(Y_e) G(Y_e | Y_{e,c}, \Delta Y_e^2) dY_e, \quad (2)$$

where  $Y_i(Y_e)$  is the abundance of the  $i$ th nuclide in a given  $Y_e$  and  $G(Y_e | Y_{e,c}, \Delta Y_e^2)$  is the normalized Gaussian distribution. We take  $Y_{e,c} = 0.15$  for dynamical ejecta and  $Y_{e,c} = 0.30$  for wind ejecta. The width of the Gaussian distribution is set to be  $\Delta Y_e = 0.04$  (Wu et al. 2019b).

Figure 1 shows the resulting abundance patterns from  $r$ -process nucleosynthesis simulations. It is found that the dynamical ejecta is sufficiently neutron rich and produces a wide range of elements from the second to third  $r$ -process peak. For a high- $Y_e$  wind ejecta, the  $r$ -process is not fully proceeded and the nuclides around the first and second  $r$ -process peaks are produced. It is known that the elemental abundances in some  $r$ -process enriched halo stars show remarkable agreement with the Solar  $r$ -process residuals, where the contribution of the  $s$ -process is subtracted (Snedden et al. 2008; Roederer 2017; Thielemann et al. 2017; Beniamini et al. 2018). This fact suggests that a single phenomenon reproduces the solar-like  $r$ -process abundance patterns. Hence we take the Solar  $r$ -process residuals from Arnould et al. (2007) for a comparison. One can observe that the neutron star merger reproduces the main features of the Solar  $r$ -process residuals. If the nucleosynthesis yields in AT2017gfo can be taken as typical for neutron star mergers, together with the merger rate of  $R_{\text{BNS}} = 1540^{+3200}_{-1220} \text{ Gpc}^{-3} \text{ yr}^{-1}$  inferred from the LIGO/Virgo discovery (Abbott et al. 2017a), one obtains that neutron star mergers are major sources of  $r$ -process elements in our Galaxy and Solar System (Siegel et al. 2019).

To explore the effects of nuclear physics inputs on the  $r$ -process nucleosynthesis simulations, we estimate the abundance patterns by using the nuclear masses from the Duflo-Zuker model (DZ, Duflo & Zuker 1995) and the fission reactions from the symmetric split model (SS, Lippuner & Roberts 2015). The results are shown in Figure 1. It is found that for a high- $Y_e$  wind ejecta, the abundance pattern is similar for different nuclear physics inputs. This is reasonable since the  $r$ -process path are close to the valley of stability, where the discrepancies between the masses predicted by different nuclear mass models are modest. For a neutron-rich dynamical ejecta, the  $r$ -process proceeds past the third  $r$ -process peak and the fission properties play a key role in shaping the abundance patterns. Thus, the abundance patterns calculated with the double Gaussian fission model have a broader second  $r$ -process peak since its fission products is in a wider range.

### 2.3. Gamma-Ray Photon Opacity

To calculate the radioactively-powered GRTs from neutron star mergers, we need to consider the effect of absorption and scattering by the ejected material. The gamma-ray photons released by radioactive decay of unstable nuclei are in the energy range from a few keV to  $\sim 3$  MeV. These MeV gamma-ray photons may interact with matter by three main mechanisms: photoelectric absorption, Compton scattering, and pair production. In the photoelectric absorption process, the gamma-ray photon loses all of its energy in one interaction. The probability for this process sensitively depends on gamma-ray energy  $E_\gamma$

and atomic number  $Z$ . In Compton scattering, the gamma-ray photon loses only part of its energy in one interaction. The probability for this process is weakly dependent on  $E_\gamma$  and  $Z$ . The gamma-ray photon can lose all of its energy in one pair production interaction. The three interaction processes described above all contribute to the opacity of merger ejecta.

We extract the opacity values of all elements from the XCOM database published by the National Institute of Standards and Technology (NIST) website<sup>1</sup>. The opacity curves of the elements from hydrogen ( $Z = 1$ ) to fermium ( $Z = 100$ ) at energies between 1 keV and 100 MeV are shown in Figure 2. As the photon energy increases, the dominant interaction mechanism shifts from photoelectric absorption to Compton scattering to pair production. For gamma-ray energies below 500 keV, photoelectric absorption is the dominant process. The probability for this process increases significantly for high- $Z$  elements. For gamma-ray photons at energies between 500 keV and 5 MeV, Compton scattering becomes the dominant interaction in matter. The probability for this process is weakly dependent on  $Z$  and the opacity curves for all elements are nearly identical. Pair production can occur with gamma-ray energies exceeding 1.022 MeV and become a significant process at energies over 5 MeV.

We calculate the opacities of ejected material based on the detailed nuclide composition, i.e.

$$\kappa_\gamma(E_\gamma) = \sum_i A_i Y_i(t) \kappa_i(E_\gamma), \quad (3)$$

where  $A_i$  is the atomic mass number of the  $i$ th nuclide,  $Y_i(t)$  is the corresponding abundance, and  $\kappa_i(E_\gamma)$  is the opacity of the  $i$ th nuclide. In Figure 2, we show the opacities of the dynamical and wind ejecta, where dashed line shows the opacity of the iron element. We find that the opacities are higher than that of the iron element in the sub-MeV energy range by a factor of  $\sim 4$  in the dynamical ejecta and  $\sim 2$  in the wind ejecta. In particular, as shown in Figure 2, the opacity of the dynamical ejecta is higher than that of the iron element by roughly an order of magnitude for photons at energy around 100 keV. This is because the probability of photoelectric absorption process is substantially enhanced by high- $Z$  elements. For photon energy  $\gtrsim 1$  MeV, the opacities of the dynamical and wind ejecta are very similar and vary relatively slowly with photon energy.

---

<sup>1</sup><https://www.nist.gov/pml/xcom-photon-cross-sections-database>

### 3. Radioactively-Powered Gamma-Ray Transients

#### 3.1. GRT Model

Our calculations of radioactively-powered GRTs are implemented based on a radiation transfer model reported in [Chen et al. \(2021\)](#). The gamma-ray energy generation rate is given by summing the energy generation of all decay mode for all nuclides, i.e.,

$$\dot{E}_\gamma = N_B \sum_i Y_i(t) \sum_j \frac{\epsilon_{ij}}{\tau_{ij}}, \quad (4)$$

where  $N_B$  is the total number of baryons,  $\epsilon_{ij}$  is the total energy of the gamma rays generated in the  $j$ th decay mode of the  $i$ th nuclide, and  $\tau_{ij}$  is the mean lifetime. The gamma-ray radiation data in each decay mode (including the  $\alpha$ -decay and  $\beta$ -decay) are taken from the NuDat2 database at the National Nuclear Data Center<sup>2</sup>.

To obtain the emitted gamma rays from the ejecta, we solve the radiative transfer equation to get the emission intensity  $I_E$ , i.e.,

$$\frac{dI_E}{dl} = -\alpha(E_\gamma)I_E + j_E, \quad (5)$$

where  $\alpha(E_\gamma)$  is the absorption coefficient,  $j_E$  is the emission coefficient, and  $l$  is the photon path length. For the gamma-ray photons travel from  $l_0$  to  $l_m$ , we can get the intensity  $I_E$  to be

$$I_E = I_E(l_0)e^{(-\tau(l_m)-\tau(l_0))} + \int_{l_0}^{l_m} j_E e^{(-\tau(l_m)-\tau(l))} dl, \quad (6)$$

where the optical depth  $\tau(l)$  is given by  $\tau(l) = \int \alpha(E_\gamma) dl$ . Here we use the analytic formulas for optical depth as described in [Chen et al. \(2021\)](#). Then the observed flux contributed by the  $n$ th layer can be obtained by

$$F_n = \int I_E \cos \theta d\Omega \approx 2\pi \int_0^\theta I_E \theta d\theta, \quad (7)$$

where  $\theta$  is the angle between line of sight and the line between ejecta centre and observer. The total observed photon flux produced by the radioactive decay of  $r$ -process elements can be obtained by summarizing the contributions of all layers,

$$F_\gamma = \sum_n F_n. \quad (8)$$

---

<sup>2</sup><http://www.nndc.bnl.gov/nudat2/>



### 3.2. Numerical Results

Figure 3 shows the gamma-ray energy generation rates for the dynamical and wind ejecta, where the dotted line indicates the power-law energy generation rate, i.e.,  $\dot{E}_\gamma = 10^{10} t_d^{-1.3} \text{ erg s}^{-1} \text{ g}^{-1}$ , where  $t_d$  is the time after the merger in days. One can observe that the gamma-ray energy generation rate of the wind ejecta can be roughly described with a power-law function. For the dynamical ejecta, a “bump” feature is shown at several days after the merger. We calculate the generated gamma-ray energy of each nuclide in the dynamical ejecta and find that the bump feature is dominated by  $^{132}\text{I}$  since the radioactive decay of  $^{132}\text{I}$  releases  $\sim 2260$  keV gamma-ray energy per decay, being higher by a factor of  $\sim 3$  than the mean gamma-ray energy (710 keV) of 1309 nuclide species in NuDat2 database.

In Figure 3, we also show the gamma-ray energy generation rates calculated with different nuclear physics inputs. For a high- $Y_e$  wind ejecta, the gamma-ray energy generation rates are similar for different nuclear physics inputs due to their similar abundance pattern. The gamma-ray energy generation rates in the dynamical ejecta are sensitive to the nuclear physics inputs. This is owing to that the dominant contributors of gamma-ray energy in the dynamical ejecta are the nuclides around the second  $r$ -process peak (Chen et al. 2021), which is sensitive to the nuclear physics models.

Figures 4 and 5 show the derived GRT lightcurves and spectra of the dynamical and wind ejecta from our model by varying the ejecta mass from  $0.001$  to  $0.05M_\odot$  (with increment of  $0.001M_\odot$ ) and velocity from  $0.1$  to  $0.4c$  (with increment of  $0.01c$ ). One can observe that the peak time and peak luminosity of the GRT lightcurves of the dynamical and wind ejecta are almost the same due to their similar gamma-ray energy generation rates. The GRT lightcurves of both the dynamical and wind ejecta are sensitive to the mass and the velocity. The GRT lightcurve of an ejecta with higher mass have a higher peak luminosity, peaks at later time, and lasts longer for a given  $v_{\text{ej}}$ . Their peak luminosities vary from  $10^{40} \sim 10^{42} \text{ erg s}^{-1}$ . The early GRT lightcurve ( $t \lesssim 3$  days) is sensitive to  $v_{\text{ej}}$ , but it is degenerated at the late time for different  $v_{\text{ej}}$ . This is reasonable since the ejecta at the peak time is almost transparent to gamma-ray photons, and the lightcurves for different velocities tend to be degenerated due to their same ejecta mass. The dependence of the GRT peak time and peak luminosity generally follows the relations

$$t_{\text{pk}} \approx 0.9 \text{ days} \left( \frac{M_{\text{ej}}}{0.01M_\odot} \right)^{1/2} \left( \frac{v_{\text{ej}}}{0.2c} \right)^{-1}, \quad (9)$$

$$L_{\text{pk}} \approx 7.0 \times 10^{40} \text{ erg s}^{-1} \left( \frac{M_{\text{ej}}}{0.01M_\odot} \right)^{1/2} \left( \frac{v_{\text{ej}}}{0.2c} \right). \quad (10)$$

The energy flux spectra of the dynamical and wind ejecta at  $t = 1$  day are shown in



Figure 5. The black lines in each panel indicate the gamma-ray lines at the rest frame and  $M_{\text{ej}}$  is set to  $0.01M_{\odot}$ . The energies of emitted gamma-ray photons are typically in a range from  $0.2 - 3$  MeV, and most of the gamma-ray photons are at energies of  $\sim 800$  keV. The low-energy ( $E_{\gamma} \lesssim 200$  keV) gamma-ray photons seriously suffer the photoelectric absorption by high- $Z$  elements in the ejecta (as discussed in Section 2.3) and only the gamma rays emitted from the near side of sphere can be seen. From Figure 5 we see that the spectrum of an ejecta with higher mass have a larger energy flux. The peak fluxes at  $\sim 800$  keV vary from  $10^{-13}$  to  $10^{-11}$  erg cm $^{-2}$  s $^{-1}$ . A higher expansion velocity leads to a flatter spectrum due to the Doppler broadening effect.

The nuclear physics inputs may affect the magnitude and shape of the gamma-ray spectrum. To explore the sensitivity to the nuclear physics inputs, we calculate the energy flux spectra by using different nuclear mass models and fission fragment distributions. Our results are shown in Figure 6, where properties of the merger ejecta are taken as  $M_{\text{ej}} = 0.0065M_{\odot}$ ,  $v_{\text{ej}} = 0.2c$ , and  $Y_{\text{e}} = 0.05$ , which is similar to the basic compositions used in [Korobkin et al. \(2020\)](#). It is found that the spectra calculated by using different nuclear physics have very similar magnitude and shapes, although the peak fluxes have some subtle differences. We note that our calculation assumed a spherical expanding ejecta model, which may cause an underestimate of the gamma-ray emission. Recently, [Korobkin et al. \(2020\)](#) applied an axisymmetric model in the gamma-ray spectrum calculations (see their Figure 4). In Figure 6, we compare our resulting spectra to those calculated using axisymmetric model from [Korobkin et al. \(2020\)](#). The distance is rescaled to the host galaxy of GW170817, i.e.,  $D = 40$  Mpc. One can observe that the energy flux spectra calculated by using a spherical symmetric model and an axisymmetric model have similar global shapes. The spectral peak around 800 keV is also showed in the results of [Korobkin et al. \(2020\)](#). The non-spherical geometry of ejecta produces a slightly larger flux than that of the spherical geometry.

#### 4. Application to Kilonova AT2017gfo

Kilonova AT2017gfo provides a solid case for studying its associated GRT. We apply our GRT model to this unique case. To estimate the GRT of the merger event like AT2017gfo, one should know the ejecta parameters, i.e., ejecta mass and expansion velocity. Several groups found that the lightcurve of kilonova AT2017gfo is well fit with the two component model, and derive  $M_{\text{ej}} \sim 0.025M_{\odot}$  and  $v_{\text{ej}} \sim 0.3c$  for the wind ejecta and  $M_{\text{ej}} \sim 0.035M_{\odot}$  and  $v_{\text{ej}} \sim 0.1c$  for the dynamical ejecta ([Arcavi et al. 2017](#); [Chornock et al. 2017](#); [Cowperthwaite et al. 2017](#); [Kasen et al. 2017](#); [Kilpatrick et al. 2017](#); [Nicholl et al. 2017](#); [Tanaka et al. 2017](#)). Alternately, [Tanvir et al. \(2017\)](#) and [Troja et al. \(2017\)](#) fitted the lightcurve of

AT2017gfo with an axisymmetric radiative transfer models from [Wollaeger et al. \(2018\)](#), yielding  $M_{\text{ej}} \sim 0.015M_{\odot}$  and  $v_{\text{ej}} \sim 0.08c$  for the wind ejecta and  $M_{\text{ej}} \sim 0.002M_{\odot}$  and  $v_{\text{ej}} \sim 0.2c$  for the dynamical ejecta. We adopt these parameter sets as inputs to calculate the spectrum of the GRT associated with AT2017gfo.

In Figure 7, we show the derived GRT associated with AT2017gfo. The energy flux spectrum is integrated over  $10^6$  s starting from 1 hour after merger. The derived spectra show several line features. The brightest one is around 800 keV, with a peak flux of  $\sim 10^{-12}$  erg cm $^{-2}$  s $^{-1}$ , which is generated by the radioactive decay of  $^{132}\text{I}$  and  $^{128}\text{Sb}$ . This gamma-ray line feature is also showed in the results of an axisymmetric model from [Korobkin et al. \(2020\)](#).

## 5. Conclusion and Discussion

We have studied the potential GRT powered by the radioactive decay of freshly-synthesized  $r$ -process elements in the ejecta of neutron star mergers with the two-component ejecta model, i.e. dynamical ejecta ( $Y_{\text{e}} \lesssim 0.25$ ) and wind ejecta ( $Y_{\text{e}} \gtrsim 0.25$ ).

Firstly, we analyze the composition and gamma-ray opacity of the ejecta. The nuclear reaction network code SkyNet is adopted to calculate the evolution of the elemental abundances. Basing on the detailed nuclide composition of the ejected material, we analyzed the gamma-ray opacities of  $r$ -process elements by considering three main mechanisms of gamma-ray photons interacting with ejected material, i.e., photoelectric absorption, Compton scattering, and pair production, since these processes sensitively depends on the gamma-ray energy  $E_{\gamma}$  and the atomic number  $Z$  of the material. We found that the opacities are higher than that of the iron element in the sub-MeV energy range by a factor of  $\sim 4$  in the dynamical ejecta (composed of the heavy  $r$ -process elements) and  $\sim 2$  in the wind ejecta (composed of the light  $r$ -process elements). This is because the probability of photoelectric absorption process is substantially enhanced by high- $Z$  elements.

Secondly, we investigate the potential GRTs based on the derived composition and gamma-ray opacity of the ejecta with the two-component model for ejecta mass and expansion velocity in the ranges of  $M_{\text{ej}} = 0.001 \sim 0.05M_{\odot}$  and  $v_{\text{ej}} = 0.1 \sim 0.4c$ . It is found that a more massive ejecta tends to power a later and brighter GRT, and a faster ejecta tends to power an earlier GRT. The dependence of the GRT peak time and peak luminosity generally follows the relation of  $t_{\text{pk}} \approx 0.9M_1^{1/2}v_2^{-1}$  days;  $L_{\text{pk}} \approx 7.0 \times 10^{40}M_1^{1/2}v_2$  erg s $^{-1}$ , where  $M_1 = M_{\text{ej}}/0.01M_{\odot}$  and  $v_2 = v_{\text{ej}}/0.2c$ . The value of  $v_{\text{ej}}$  can significantly affect the shape of the gamma-ray spectrum through the Doppler broadening effect.

Finally, as a case study, we apply our model to the possible GRT associated with AT2017gfo for evaluating its detection probability. We adopt two different sets of ejecta parameters derived by several groups: (1)  $M_{\text{ej}} = 0.025M_{\odot}$  and  $v_{\text{ej}} = 0.3c$  for the wind ejecta and  $M_{\text{ej}} = 0.035M_{\odot}$  and  $v_{\text{ej}} = 0.1c$  for the dynamical ejecta; (2)  $M_{\text{ej}} = 0.015M_{\odot}$  and  $v_{\text{ej}} = 0.08c$  for the wind ejecta and  $M_{\text{ej}} = 0.002M_{\odot}$  and  $v_{\text{ej}} = 0.2c$  for the dynamical ejecta. The derived spectra show several gamma-ray line features and the brightest one around 800 keV is generated by the radioactive decay of  $^{132}\text{I}$  and  $^{128}\text{Sb}$ . This line feature can be used as a fingerprint to probe the production of heavy elements in future gamma-ray observation.

The flux threshold of the current MeV gamma-ray mission INTEGRAL is  $5 \times 10^{-11} \text{ erg cm}^{-2} \text{ s}^{-1}$  (15 keV–8 MeV, exposure time  $10^6 \text{ s}$ , Diehl 2013), being much lower than the peak gamma-ray energy fluxes derived from our analysis. The proposed MeV gamma-ray instruments, such as ETCC (0.15–20 MeV,  $10^6 \text{ s}$  Tanimori et al. 2015) and AMEGO (0.3 MeV–10 GeV,  $10^6 \text{ s}$ , Moiseev & Amego Team 2017), have a sensitivity of  $\sim 2 \times 10^{-12} \text{ erg cm}^{-2} \text{ s}^{-1}$ , being closed to the peak gamma-ray flux of the GRT. For convincingly detecting such a GRT, the sensitivity of the instruments should be improved at least one order of magnitude. To identify the gamma-ray line features, a detector having present-level energy resolution would be most desired. The proposed gamma-ray mission AMEGO can provide  $< 1\%$  energy resolution in the MeV band but it not sensitive enough for convincing detection such a GRT.

We should emphasize that the detection of GRT event associated with AT2017gfo with ETCC and AMEGO like instruments is still over optimistic. The event rate of binary neutron star merger inferred from AT2017gfo is  $R_{\text{BNS}} = 1540_{-1220}^{+3200} \text{ Gpc}^{-3} \text{ yr}^{-1}$  (Abbott et al. 2017a). The occurrence rates within a spherical volume of radius 40 Mpc is then  $\sim 0.4_{-0.3}^{+0.9} \text{ yr}^{-1}$ . The extremely low occurrence rate and flux level make a great challenge to discover the GRT with ETCC and AMEGO like instruments. More sensitive instruments in the MeV gamma-ray band are required for increasing the detection probability of the GRT in a deeper universe.

The total ejecta mass required to fit the kilonova AT2017gfo is relatively larger than that predicted by numerical-relativity simulations for neutron star mergers ( $\lesssim 0.01M_{\odot}$ ; Nedora et al. 2021). Yu et al. (2018) suggested that the spin-down of long-lived remnant neutron star may provide extra power to the kilonova emission, and required mass of the radioactive elements is reduced. The GRT with a smaller ejecta mass should be dimmer. This also lowers down the detection probability. We should also note that the interaction between the dynamical and wind ejecta is ignored in our calculations (Kawaguchi et al. 2018). The ejecta morphology may influence the lightcurve and spectrum of radioactively-powered GRTs (Wollaeger et al. 2018; Korobkin et al. 2021).

We thank Li-Xin Li, Hou-Jun Lü, Da-Bin Lin, and Ning Wang for fruitful discussion and anonymous referee for helpful comments. This work was supported by the National Natural Science Foundation of China (grant Nos. 12133003, 11773007, and U1731239) and the Guangxi Science Foundation (grant Nos. AD17129006, 2017AD22006, 2018GXNSFFA281010, and 2018GXNSFGA281007).

## REFERENCES

- Abbott, B. P., Abbott, R., Abbott, T. D., et al. 2017, *Phys. Rev. Lett.*, 119, 161101. doi:10.1103/PhysRevLett.119.161101
- Abbott, B. P., Abbott, R., Abbott, T. D., et al. 2017, *ApJ*, 848, L12. doi:10.3847/2041-8213/aa91c9
- Arcavi, I., Hosseinzadeh, G., Howell, D. A., et al. 2017, *Nature*, 551, 64. doi:10.1038/nature24291
- Arnould, M., Goriely, S., & Takahashi, K. 2007, *Phys. Rep.*, 450, 97. doi:10.1016/j.physrep.2007.06.002
- Barnes, J. & Kasen, D. 2013, *ApJ*, 775, 18. doi:10.1088/0004-637X/775/1/18
- Barnes, J., Kasen, D., Wu, M.-R., et al. 2016, *ApJ*, 829, 110. doi:10.3847/0004-637X/829/2/110
- Bauswein, A., Goriely, S., & Janka, H.-T. 2013, *ApJ*, 773, 78. doi:10.1088/0004-637X/773/1/78
- Beniamini, P., Dvorkin, I., & Silk, J. 2018, *MNRAS*, 478, 1994. doi:10.1093/mnras/sty1035
- Burbidge, E. M., Burbidge, G. R., Fowler, W. A., et al. 1957, *Reviews of Modern Physics*, 29, 547. doi:10.1103/RevModPhys.29.547
- Chen, M.-H., Li, L.-X., Lin, D.-B., et al. 2021, *ApJ*, 919, 59. doi:10.3847/1538-4357/ac1267
- Chornock, R., Berger, E., Kasen, D., et al. 2017, *ApJ*, 848, L19. doi:10.3847/2041-8213/aa905c
- Coulter, D. A., Foley, R. J., Kilpatrick, C. D., et al. 2017, *Science*, 358, 1556. doi:10.1126/science.aap9811

- Cowperthwaite, P. S., Berger, E., Villar, V. A., et al. 2017, *ApJ*, 848, L17. doi:10.3847/2041-8213/aa8fc7
- Cyburt, R. H., Amthor, A. M., Ferguson, R., et al. 2010, *ApJS*, 189, 240. doi:10.1088/0067-0049/189/1/240
- Diehl, R. 2013, *Reports on Progress in Physics*, 76, 026301. doi:10.1088/0034-4885/76/2/026301
- Dietrich, T., Ujevic, M., Tichy, W., et al. 2017, *Phys. Rev. D*, 95, 024029. doi:10.1103/PhysRevD.95.024029
- Drout, M. R., Piro, A. L., Shappee, B. J., et al. 2017, *Science*, 358, 1570. doi:10.1126/science.aag0049
- Duflo, J. & Zuker, A. P. 1995, *Phys. Rev. C*, 52, R23. doi:10.1103/PhysRevC.52.R23
- Evans, P. A., Cenko, S. B., Kennea, J. A., et al. 2017, *Science*, 358, 1565. doi:10.1126/science.aap9580
- Fujibayashi, S., Kiuchi, K., Nishimura, N., et al. 2018, *ApJ*, 860, 64. doi:10.3847/1538-4357/aabafd
- Goriely, S., Hilaire, S., & Koning, A. J. 2008, *A&A*, 487, 767. doi:10.1051/0004-6361:20078825
- Hotokezaka, K., Kiuchi, K., Kyutoku, K., et al. 2013, *Phys. Rev. D*, 88, 044026. doi:10.1103/PhysRevD.88.044026
- Hotokezaka, K., Wanajo, S., Tanaka, M., et al. 2016, *MNRAS*, 459, 35. doi:10.1093/mnras/stw404
- Kasen, D., Badnell, N. R., & Barnes, J. 2013, *ApJ*, 774, 25. doi:10.1088/0004-637X/774/1/25
- Kasen, D., Metzger, B., Barnes, J., et al. 2017, *Nature*, 551, 80. doi:10.1038/nature24453
- Kasliwal, M. M., Nakar, E., Singer, L. P., et al. 2017, *Science*, 358, 1559. doi:10.1126/science.aap9455
- Kawaguchi, K., Shibata, M., & Tanaka, M. 2018, *ApJ*, 865, L21. doi:10.3847/2041-8213/aade02
- Kilpatrick, C. D., Foley, R. J., Kasen, D., et al. 2017, *Science*, 358, 1583. doi:10.1126/science.aag0073

- Kodama, T. & Takahashi, K. 1975, Nucl. Phys. A, 239, 489. doi:10.1016/0375-9474(75)90381-4
- Kondey, F. G., Wang, M., Huang, W.-J., et al. 2021, Chinese Physics C, 45, 030001. doi:10.1088/1674-1137/abddae
- Korobkin, O., Rosswog, S., Arcones, A., et al. 2012, MNRAS, 426, 1940. doi:10.1111/j.1365-2966.2012.21859.x
- Korobkin, O., Hungerford, A. M., Fryer, C. L., et al. 2020, ApJ, 889, 168. doi:10.3847/1538-4357/ab64d8
- Korobkin, O., Wollaeger, R. T., Fryer, C. L., et al. 2021, ApJ, 910, 116. doi:10.3847/1538-4357/abe1b5
- Lattimer, J. M. & Schramm, D. N. 1974, ApJ, 192, L145. doi:10.1086/181612
- Li, L.-X. & Paczyński, B. 1998, ApJ, 507, L59. doi:10.1086/311680
- Li, L.-X. 2019, ApJ, 872, 19. doi:10.3847/1538-4357/aaf961
- Lippuner, J. & Roberts, L. F. 2015, ApJ, 815, 82. doi:10.1088/0004-637X/815/2/82
- Lippuner, J. & Roberts, L. F. 2017, ApJS, 233, 18. doi:10.3847/1538-4365/aa94cb
- Metzger, B. D., Martínez-Pinedo, G., Darbha, S., et al. 2010, MNRAS, 406, 2650. doi:10.1111/j.1365-2966.2010.16864.x
- Metzger, B. D. 2019, Living Reviews in Relativity, 23, 1. doi:10.1007/s41114-019-0024-0
- Moiseev, A. & Amego Team 2017, 35th International Cosmic Ray Conference (ICRC2017), 301, 798
- Möller, P., Sierk, A. J., Ichikawa, T., et al. 2016, Atomic Data and Nuclear Data Tables, 109, 1. doi:10.1016/j.adt.2015.10.002
- Mumpower, M. R., Kawano, T., Sprouse, T. M., et al. 2018, ApJ, 869, 14. doi:10.3847/1538-4357/aaeaca
- Nedora, V., Bernuzzi, S., Radice, D., et al. 2021, ApJ, 906, 98. doi:10.3847/1538-4357/abc9be
- Nicholl, M., Berger, E., Kasen, D., et al. 2017, ApJ, 848, L18. doi:10.3847/2041-8213/aa9029
- Pian, E., D’Avanzo, P., Benetti, S., et al. 2017, Nature, 551, 67. doi:10.1038/nature24298

- Radice, D., Perego, A., Hotokezaka, K., et al. 2018, *ApJ*, 869, 130. doi:10.3847/1538-4357/aaf054
- Roederer, I. U. 2017, *ApJ*, 835, 23. doi:10.3847/1538-4357/835/1/23
- Sekiguchi, Y., Kiuchi, K., Kyutoku, K., et al. 2016, *Phys. Rev. D*, 93, 124046. doi:10.1103/PhysRevD.93.124046
- Shibata, M. & Hotokezaka, K. 2019, *Annual Review of Nuclear and Particle Science*, 69, 41. doi:10.1146/annurev-nucl-101918-023625
- Siegel, D. M., Barnes, J., & Metzger, B. D. 2019, *Nature*, 569, 241. doi:10.1038/s41586-019-1136-0
- Smartt, S. J., Chen, T.-W., Jerkstrand, A., et al. 2017, *Nature*, 551, 75. doi:10.1038/nature24303
- Snedden, C., Cowan, J. J., & Gallino, R. 2008, *ARA&A*, 46, 241. doi:10.1146/annurev.astro.46.060407.145207
- Tanaka, M., Utsumi, Y., Mazzali, P. A., et al. 2017, *PASJ*, 69, 102. doi:10.1093/pasj/psx121
- Tanimori, T., Kubo, H., Takada, A., et al. 2015, *ApJ*, 810, 28. doi:10.1088/0004-637X/810/1/28
- Tanvir, N. R., Levan, A. J., González-Fernández, C., et al. 2017, *ApJ*, 848, L27. doi:10.3847/2041-8213/aa90b6
- Thielemann, F.-K., Eichler, M., Panov, I. V., et al. 2017, *Annual Review of Nuclear and Particle Science*, 67, 253. doi:10.1146/annurev-nucl-101916-123246
- Troja, E., Piro, L., van Eerten, H., et al. 2017, *Nature*, 551, 71. doi:10.1038/nature24290
- Villar, V. A., Guillochon, J., Berger, E., et al. 2017, *ApJ*, 851, L21. doi:10.3847/2041-8213/aa9c84
- Wang, M., Huang, W.-J., Kondev F. G., et al. 2021, *Chinese Physics C*, 45, 030003. doi:10.1088/1674-1137/abddaf
- Watson, D., Hansen, C. J., Selsing, J., et al. 2019, *Nature*, 574, 497. doi:10.1038/s41586-019-1676-3
- Wollaeger, R. T., Korobkin, O., Fontes, C. J., et al. 2018, *MNRAS*, 478, 3298. doi:10.1093/mnras/sty1018



- Wu, M.-R., Banerjee, P., Metzger, B. D., et al. 2019, *ApJ*, 880, 23. doi:10.3847/1538-4357/ab2593
- Wu, M.-R., Barnes, J., Martínez-Pinedo, G., et al. 2019, *Phys. Rev. Lett.*, 122, 062701. doi:10.1103/PhysRevLett.122.062701
- Yu, Y.-W., Liu, L.-D., & Dai, Z.-G. 2018, *ApJ*, 861, 114. doi:10.3847/1538-4357/aac6e5
- Zhu, Y. L., Lund, K. A., Barnes, J., et al. 2021, *ApJ*, 906, 94. doi:10.3847/1538-4357/abc69e

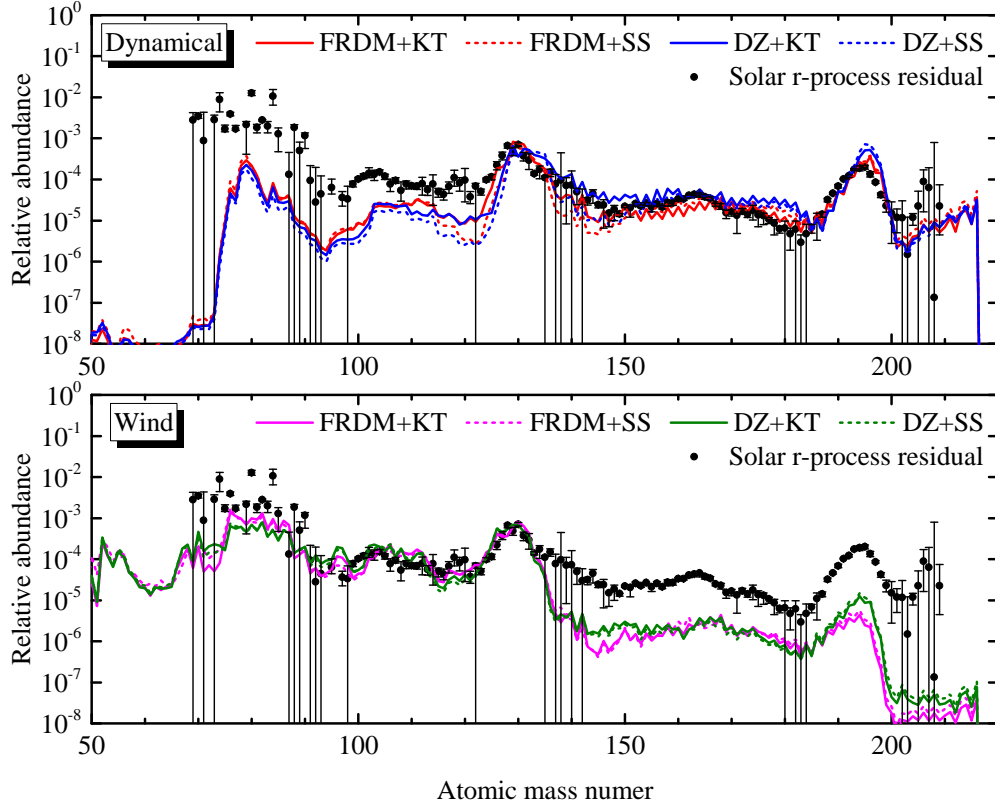


Fig. 1.— Abundance patterns of  $r$ -process element for dynamical and wind ejecta at  $t = 10^9$  s. The solar  $r$ -process abundance taken from (Arnould et al. 2007) is shown with black dots for comparison. FRDM = Finite-Range Droplet Model; DZ = Duflo-Zuker model; KT = Kodama-Takahashi fission model; SS = symmetric split model.

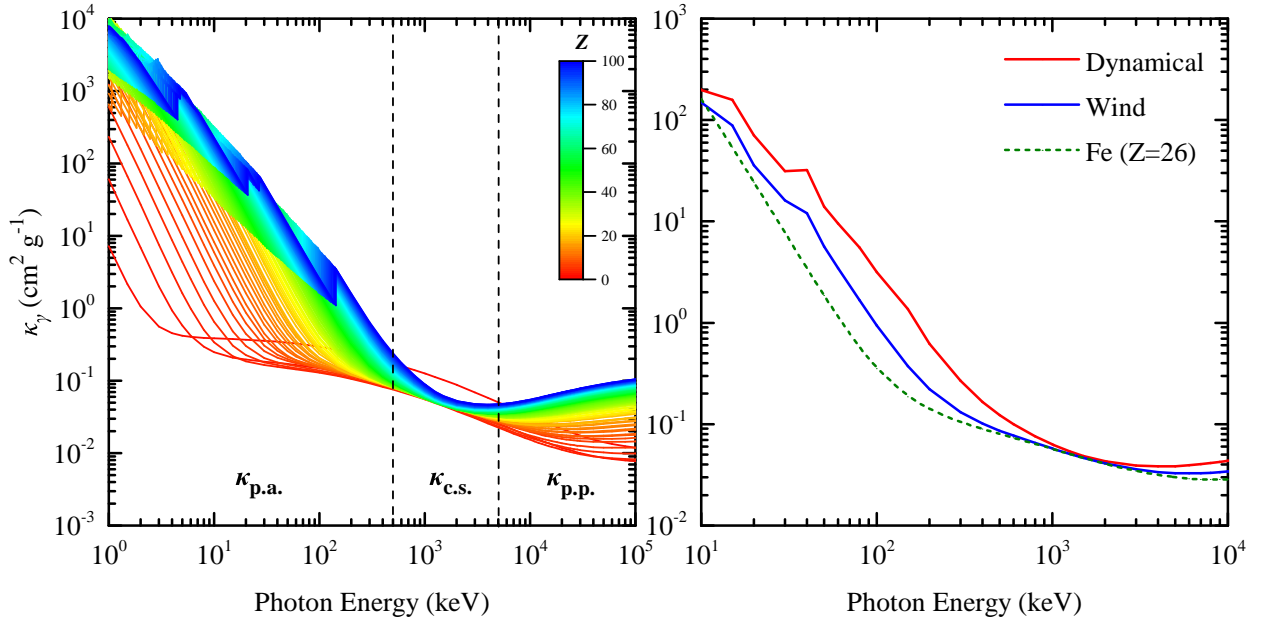


Fig. 2.— Gamma-ray photon opacity as a function of photon energy for individual elements from hydrogen ( $Z = 1$ ) to fermium ( $Z = 100$ ) (left panel) and for the wind and dynamical ejecta (right panel). The gamma-ray opacity of the iron element is also shown with a dashed line in the right panel for comparison. The opacity is calculated by considering the photoelectric absorption ( $\kappa_{\text{p.a.}}$ ), Compton scattering ( $\kappa_{\text{c.s.}}$ ), and pair production ( $\kappa_{\text{p.p.}}$ ) for the gamma-rays. The opacity values of these processes are taken from XCOM database.

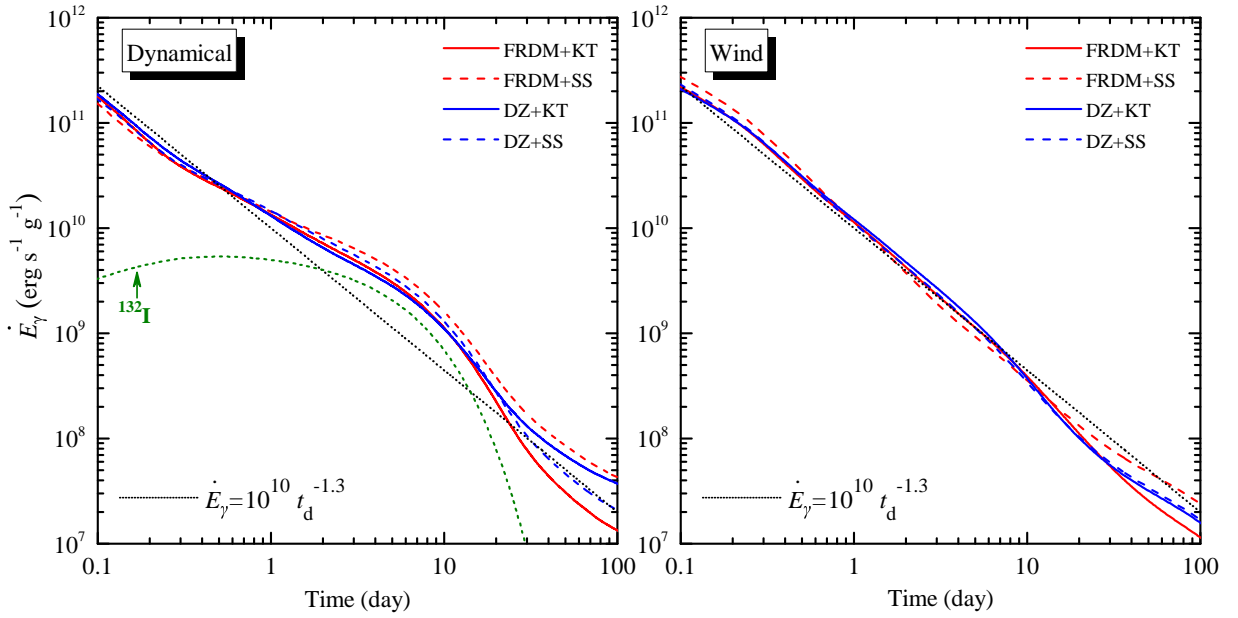


Fig. 3.— Gamma-ray energy generation rates of the dynamical and wind ejecta. The dotted lines indicate the power-law gamma-ray energy generation rate, i.e.,  $\dot{E}_\gamma = 10^{10} t_d^{-1.3} \text{ erg s}^{-1} \text{ g}^{-1}$  ( $t_d$  is the time after the merger in days). Green dashed line show the contribution from the  $\beta$ -decay of  $^{132}\text{I}$ .

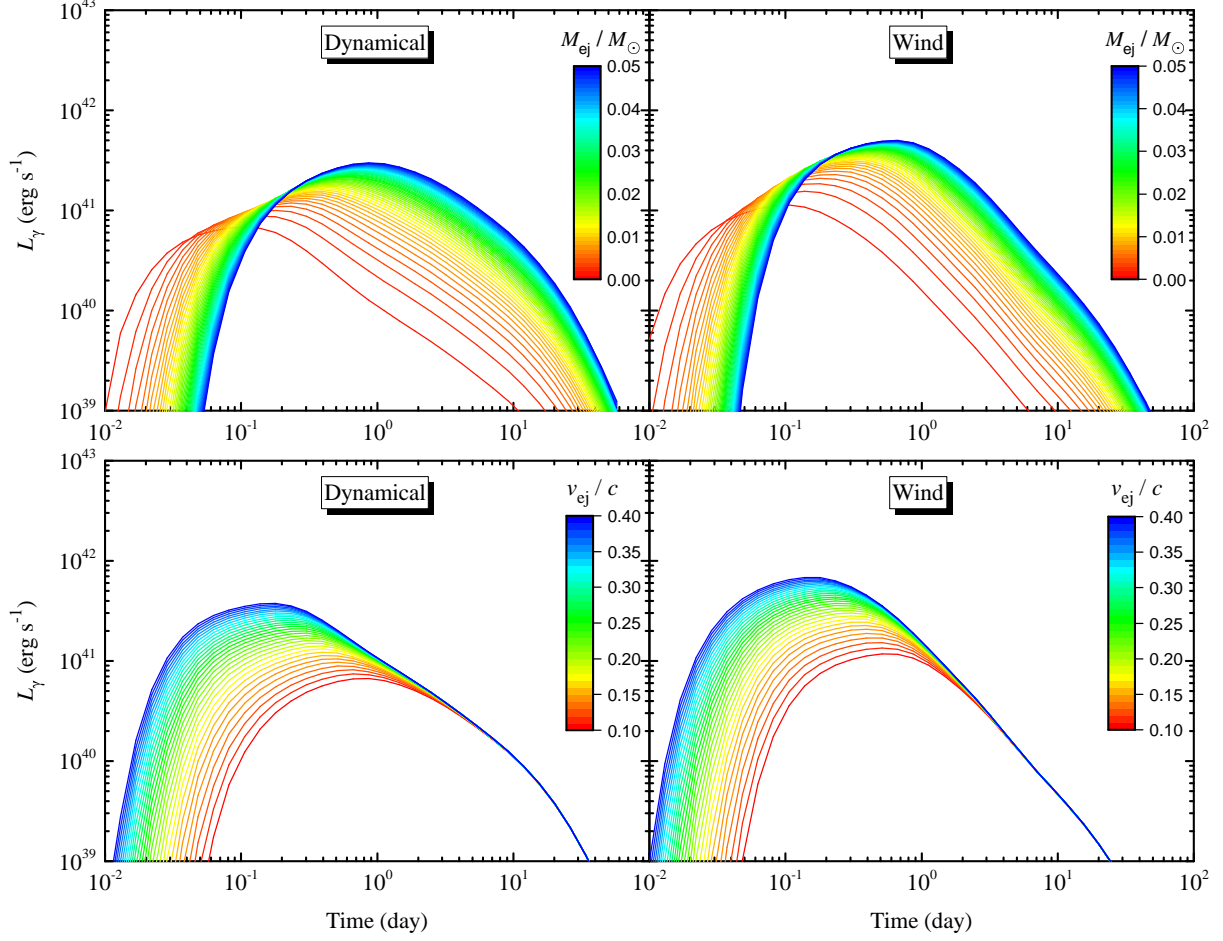


Fig. 4.— Radioactively-powered GRT lightcurves of the dynamical and wind ejecta by varying the ejecta mass from  $0.001$  to  $0.05M_{\odot}$  (with increment of  $0.001M_{\odot}$ ) and setting the ejecta expansion velocity at  $v_{\text{ej}} = 0.2c$  (top two panels) and by varying the expansion velocities from  $0.1$  to  $0.4c$  (with increment of  $0.01c$ ) and setting the ejecta mass at  $M_{\text{ej}} = 0.01M_{\odot}$  (bottom two panels).

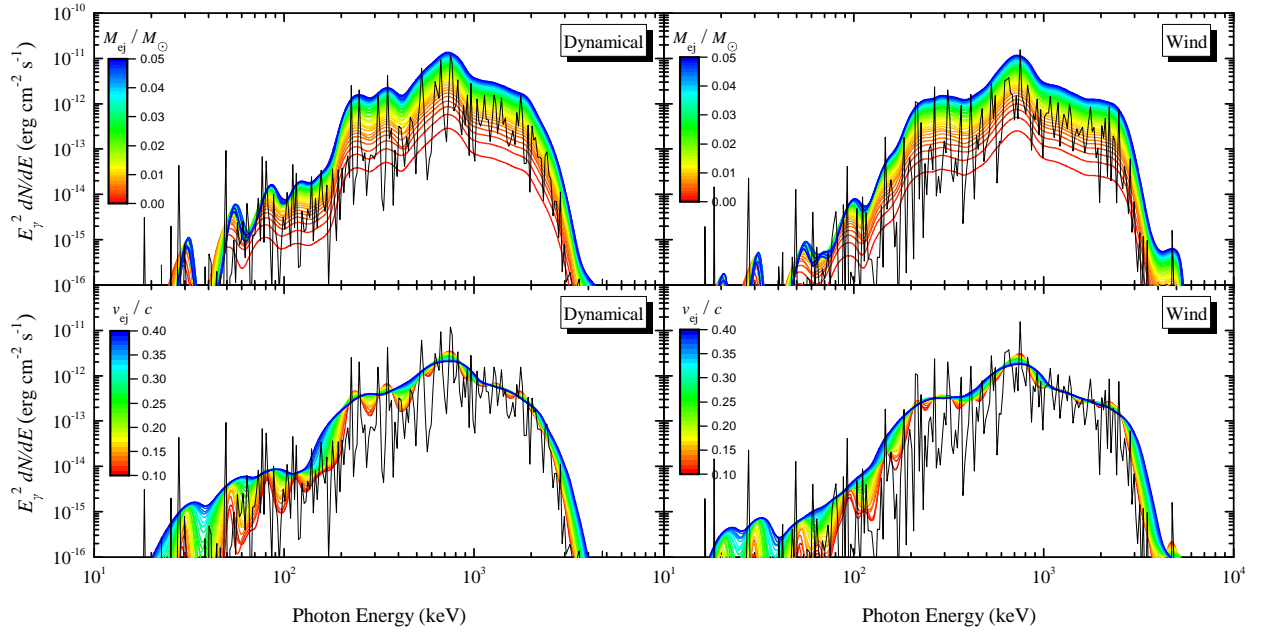


Fig. 5.— The same as Figure 4, but for the energy flux spectra at  $t = 1$  day. Black lines indicate the spectrum produced by the radioactive decay of  $r$ -process elements at the rest frame and  $M_{\text{ej}}$  is set to  $0.01 M_\odot$ . Distance to the source is 40 Mpc.

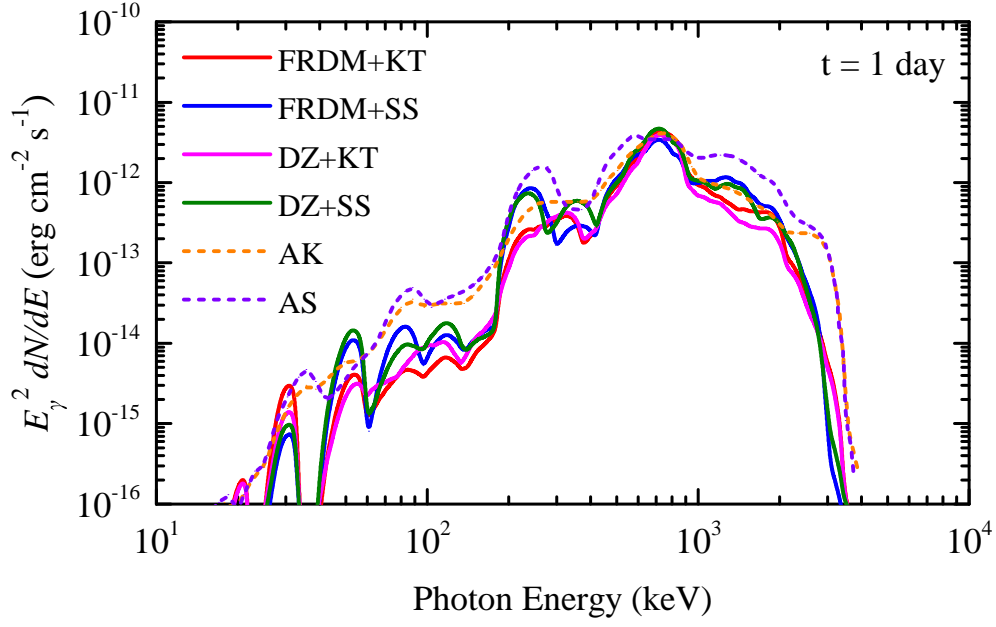


Fig. 6.— The energy flux spectra calculated with different nuclear physics inputs as marked with different color solid lines in the figure, assuming the ejecta parameters as  $M_{\text{ej}} = 0.0065 M_{\odot}$ ,  $v_{\text{ej}} = 0.2c$ , and  $Y_e = 0.05$ , which are similar to the basic composition used in [Korobkin et al. \(2020\)](#). The results for axisymmetric configuration models taken from [Korobkin et al. \(2020\)](#) are also presented with dashed lines, where “AS” is for the axisymmetric plus symmetric split fission model and “AK” is for the axisymmetric plus Kodama-Takahashi fission model. The distance is scaled to the host galaxy of GW170817, i.e.,  $D = 40$  Mpc.



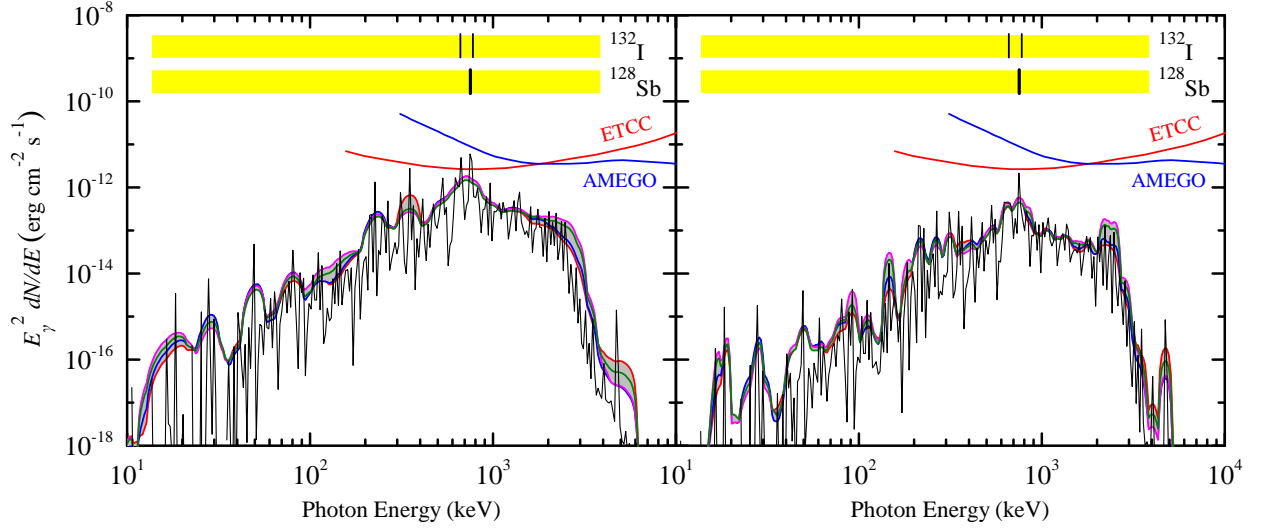


Fig. 7.— The energy flux spectra associated with AT2017gfo derived from our model by adopting ejecta parameters as: *Left panel* —  $M_{\text{ej}} = 0.025M_{\odot}$  and  $v_{\text{ej}} = 0.3c$  for the wind ejecta and  $M_{\text{ej}} = 0.035M_{\odot}$  and  $v_{\text{ej}} = 0.1c$  for the dynamical ejecta; *Right panel* —  $M_{\text{ej}} = 0.015M_{\odot}$  and  $v_{\text{ej}} = 0.08c$  for the wind ejecta and  $M_{\text{ej}} = 0.002M_{\odot}$  and  $v_{\text{ej}} = 0.2c$  for the dynamical ejecta. The spectra are integrated over the first  $10^6$  s. The grey band shows the range of resulting gamma-ray spectra from all our nuclear physics inputs. The sensitivity curves (exporsure time of  $10^6$  seconds) of ETCC and AMEGO taken from [Tanimori et al. \(2015\)](#) and [Moiseev & Amego Team \(2017\)](#) are plot for examining the delectability of the spectra with these proposed MeV gamma-ray missions. The dominant nuclide species ( $^{132}\text{I}$  and  $^{128}\text{Sb}$ ) responsible for the line feature at around 800 keV are also shown.